Vol 11 No 5, May 2002
1009-1963/2002/11(05)/0472-09

Chinese Physics

© 2002 Chin. Phys. Soc.
and IOP Publishing Ltd

Arrays of microscopic magnetic traps for cold atoms and their applications in atom optics*

Yin Jian-Ping(印建平)[a)b)], Gao Wei-Jian(高伟建)[b)], and Hu Jian-Jun(胡建军)[b)]

[a)] *Key Laboratory for Optical and Magnetic Resonance Spectroscopy and Department of Physics, East China Normal University, Shanghai 200062, China*

[b)] *Department of Physics, Suzhou University, Suzhou 215006, China*

(Received 10 June 2001; revised manuscript received 23 December 2001)

A single microscopic magnetic trap for neutral atoms using planar current-carrying wires was proposed and studied theoretically by Weinstein *et al.* In this paper, we propose three structures of composite current-carrying wires to provide 1D, 2D and 3D arrays of microscopic magnetic traps for cold alkali atoms. The spatial distributions of magnetic fields generated by these structures are calculated and the field gradient and curvature in each single microtrap are analysed. Our study shows that arrays of microscopic magnetic traps can be used to provide 1D, 2D or 3D atomic magnetic lattices, and even to realize 1D, 2D and 3D arrays of magneto-optical traps, and so on.

Keywords: magnetic micro-trap array, current-carrying wire array, atomic magnetic lattices
PACC: 3280P, 0375B, 3380P, 4250

1. Introduction

In recent years, the investigation of atomic optical lattices (AOLs),[1] i.e. arrays of microscopic optical traps composed of a lD, 2D or 3D standing laser wave, has become a hot research subject in atomic physics and atom optics. In the AOL, the interaction of an ultracold atomic gas with a spatially modulated light field can be used to confine the cold atoms at the potential maxima in red-detuned lattices or at the potential minima in blue-detuned lattices. The AOL provides a new and precise way to manipulate and control neutral atoms, adequate for studying some fundamental physical problems. So the AOL has been widely applied in the studies of ferromagnetic,[2] antiferromagnetic and paramagnetic properties,[3,4] Sisyphus cooling, polarization gradient cooling and trapping dynamics,[5,6] Raman and adiabatic cooling,[7,8] wave-packet dynamics,[9] Rabi and Bloch oscillations,[10,11] and quantum transport and tunnelling dynamics[12,13] of trapped atoms as well as Bragg diffraction of light in optical lattices,[14] and so on. However, since there are relatively strong photon-scattering effects and radiative repulsion and photon-associated collisions in the far-red-detuned optical lattices, the mean number of atoms trapped at each lattice site (that is, in each microscopic optical trap) will be limited to less than unity (say ~0.44 atom per site[15]), which results in a relatively small difference of refraction indices in the optical lattices.

In this paper, instead of the AOLs, 1D, 2D and 3D arrays of microscopic magnetic traps (MMTs) for cold atoms are proposed for the construction of atomic magnetic lattices (AMLs). The most promising features of the latter is the elimination of the unfavourable effects of spontaneous emitting, photon scattering and photon-associated collision losses in the former, so that the number of trapped atoms at each lattice site will be far larger than 1, leading to a large difference of refraction indices, which is a property significantly superior to the former in many respects. The structures of the 1D, 2D and 3D arrays of MMTs, constructed on the basis of arrays of current-carrying wires, together with calculations of the magnetic field created in them, are described in section 2. In section 3, the magnetic field of a single magnetic microtrap and its gradient and curvature distributions are calculated and analysed. In section 4, the procedures of atomic loading of the MMT arrays to form AMLs are suggested, and the collision loss rates of cold atoms in the MMT (or AML) are estimated. Our main results are summarized in section 5, together with a discussion on the prospects of applications of the AMLs.

*Project supported by the National Natural Science Foundations of China (Grant Nos 69878019 and 10174050), the Natural Science Foundation of Jiangsu Province, China (Grant No DK97139), and the Natural Science Foundation of Education Bureau of Jiangsu Province, China (Grant No 00KJB140001).

2. Arrays of microscopic magnetic traps

It is well known that a planar array of N wires connected in series, carrying equal but opposite current in adjacent wires (the total current I_0 being equal to the current I in each wire), hereafter referred to as the series (planar) wire array (SWA), can be used to construct a magnetic atomic mirror,[16,17] whereas a planar array of N wires connected in parallel, carrying equal currents of the same direction in adjacent wires (the total current being I_0=NI), hereafter referred to as the parallel (planar) wire array (PWA), can be used to form a 1D array of magnetic atomic guides. Now we use these two basic types of wire arrays to construct 1D, 2D or 3D array of MMTs for cold alkali atoms.

The structure of the 1D array of MMTs for cold atoms is shown in Fig.1(a). It consists of a PWA carrying the total current NI_1, and a pair of rectangular anti-Helmholtz coils, carrying equal but opposing currents I_2, mounted cross-wire over it, as shown in the scheme. The direction (of the wires) of the PWA is along the y-axis, and the direction of the anti-Helmholtz coils is along the x-axis. The spacing of the wires in the PWA is a, and b and c are the spacing between two anti-Helmholtz coils and the height of the rectangular coils, respectively. The length of the anti-Helmholtz coils is made far greater than c. Thus a quadrupole-like configuration of magnetic field is formed at the crossing of the PWA with the coils. The symbols "$\odot$" and "$\otimes$" are used in the present and subsequent figures to denote the "tip" and "tail", respectively, of the arrows indicating the directions of current flow.

The magnetic field from a layout of current-carrying wires can be calculated by integrating the vector potential $\boldsymbol{A}(=\dfrac{\mu_0}{4\pi}\int\dfrac{\boldsymbol{J}\mathrm{d}V}{r}$, where $\boldsymbol{J}$ is the current density in free space) over elements of each wire, and applying the relation $\boldsymbol{B}=\nabla\times\boldsymbol{A}$.[18] We calculated the spatial distribution of the magnetic field in the xoy plane from the layout of current-carrying wires shown in Fig.1(a) using the vector potential $\boldsymbol{A}$, and the result is shown in Fig.1(b). It is clear that a 1D array of microscopic magnetic wells appears, which forms a 1D array of MMTs for cold, weak-field-seeking atoms. When $I_1=I_2$=0.2A, b=2a=2c=200μm, we obtained $B(x)_{\max}\geq 150\times10^{-4}$T within Δx=$x-x_0$=$\pm$45μm, $B(y)_{\max}\geq 15\times10^{-4}$T within Δy=$y-y_0=\pm100\mu$m, and $B(z)_{\max}\geq 12\times10^{-4}$T within Δz=$z-z_0=\pm50\mu$m, where (x_0, y_0, z_0) are the coordinates of each trap centre.

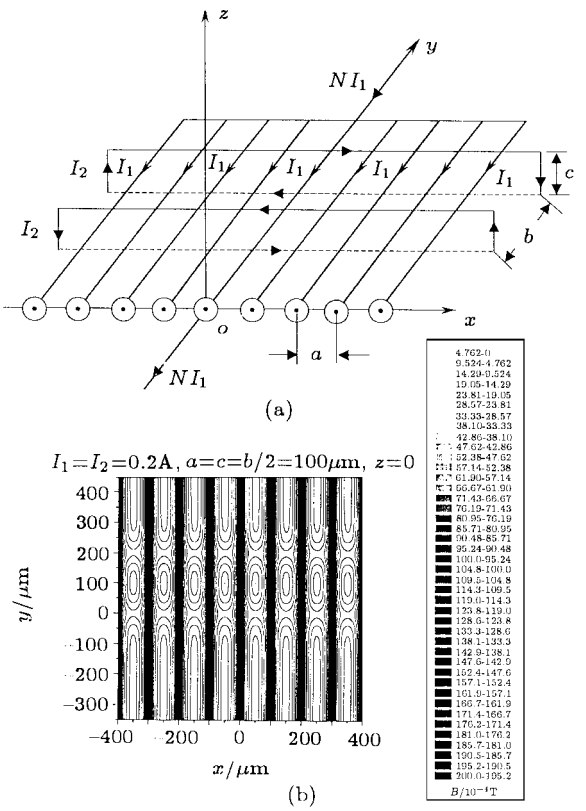


Fig.1. (a) Schematic diagram of 1D array of MMTs. (b) Magnetic field contours on the xoy plane generated by this layout, with I_1=I_2=0.2A, a=$b/2$ = c=100μm.

To construct a 2D array of MMTs, one needs only to repeat the anti-Helmholtz coils as a structure unit in the y-direction to form an array. The resulting structure turns out to be two SWAs, N wires each, say, with currents flowing in opposite directions, which enclose the PWA to form quadrupole-like configurations at the crossing, as shown in the scheme of Fig.2(a). Here b becomes the spacing of the wires in the SWAs, and c, the height of the original anti-Helmholtz coils, becomes the distance between the SWAs. We see that the structure is just a three-layer composite of the two basis types of planar wire arrays. The corresponding spatial distribution of the magnetic field in the xoy plane is shown in Fig.2(b). It is seen that there are together $N\times N$ microwells, each functioning as a micro-quadrupole-trap, and the structure as a whole forms a 2D array of MMTs for cold atoms. Our calculation shows that when I_1=I_2=0.2A, b=2a=2c=200μm, the magnetic field has the values $B(x)_{\max}\geq 150\times10^{-4}$T within Δx=$\pm$45μm, $B(y)_{\max}\geq 14\times10^{-4}$T within Δy=$\pm$100μm, and $B(z)_{\max}>12\times10^{-4}$T within Δz=$\pm$50μm.

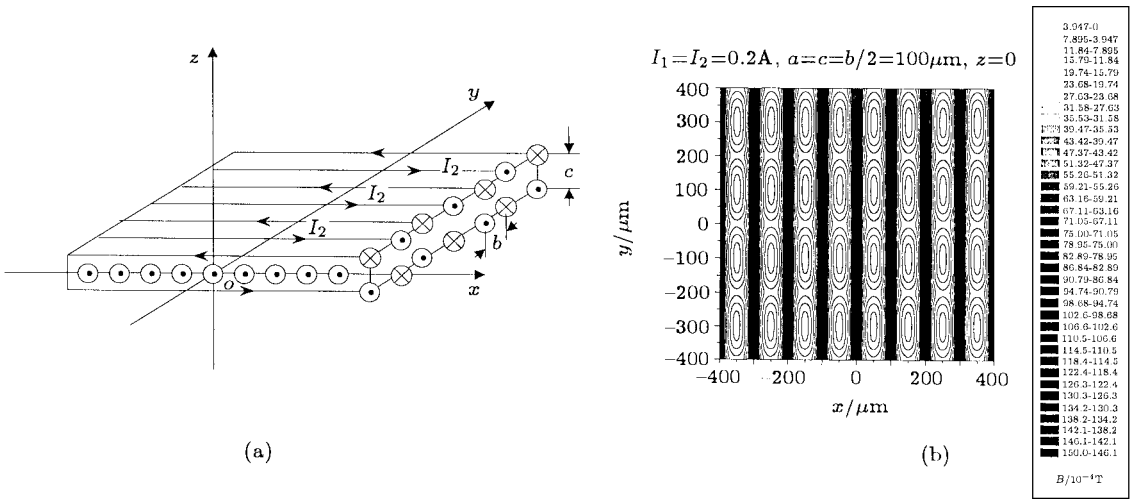


Fig.2. (a) Schematic diagram of 2D array of MMTs. (b) Magnetic field contours on the xoy plane generated by this layout, with $I_1=I_2=0.2$A, $a=b/2=c=100\mu$m..

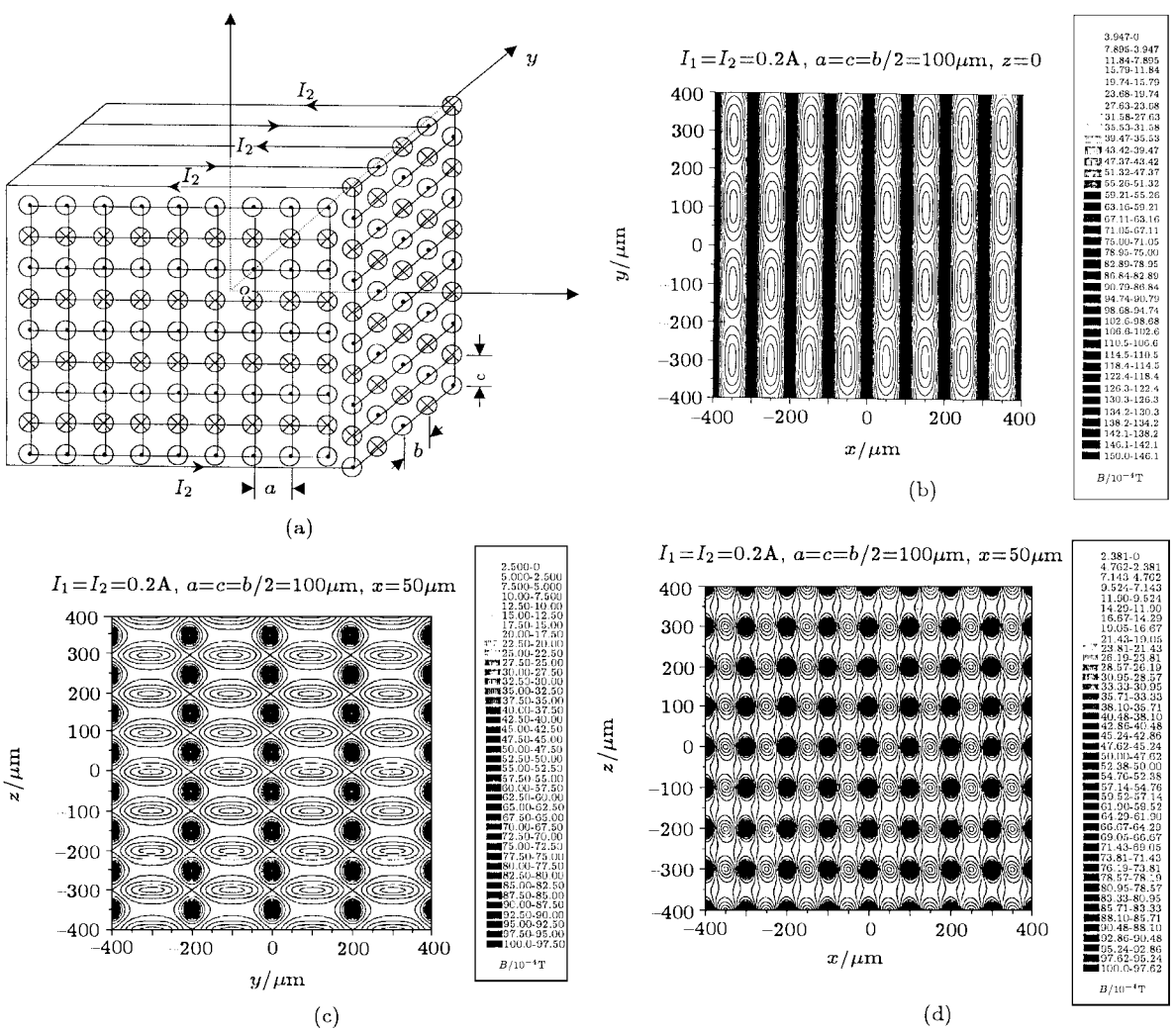


Fig.3. (a) Schematic diagram of 3D array of MMTs. Magnetic field contours on (b) the xoy plane, (c) the yoz plane, and (d) the xoz plane generated by this layout, with $I_1=I_2=0.2$A, $a=b/2=c=100\mu$m.

It is easily seen that to construct a 3D array of MMTs, one needs only to repeat the above 2D array M times, say, in the z-direction in a manner shown schematically in Fig.3(a). The resulting structure turns out to be a pile of interlacing SWAs and PWAs, carrying alternatively opposite currents in adjacent layers of each type of the wire arrays. The parameters a, b and c are essentially the same as the 2D array. The calculated results of the magnetic fields in the xoy, yoz and xoz planes are shown in Figs.3(b), (c) and (d), respectively. Again, quadrupole-like fields are formed at the crossing of each PWA with the neighbouring SWAs, resulting in a 3D array of $N \times N \times M$ microtraps. When I_1=I_2=0.2A, b=2a=2c=200μm, we obtained $B(x)_{\max} \geq 150\times10^{-4}$T within Δx=$\pm$45μm, $B(y)_{\max}$ $\geq$12$\times10^{-4}$T within Δy=$\pm$100μm, and $B(z)_{\max} \geq 10.5\times10^{-4}$T within Δz=$\pm$50μm.

3. Analysis of single microscopic magnetic well

Since the calculation method used in section 2 can only give numeric solutions of the magnetic field distributions of a single microscopic well in a 1D, 2D or 3D array of microscopic magnetic traps, which do not include any information on the effect of microstructure parameters (a, b and c) of the wire array, it is difficult to analytically calculate and analyse the relationship between the magnetic field distribution (including the gradient and curvature distribution) of a single microscopic trap and the structure parameters of the wire array. However, due to symmetry of the current distribution in the arrays of current-carrying wires, only some current-carrying wires close to each microtrap make a contribution to the magnetic field distribution of each microtrap, and this contribution can be described by an influence factor k. So the magnetic field distribution within the central area of each trap in a 1D, 2D or 3D array can be approximated by the contributions from both those current-carrying wires adjacent to each microtrap and its own quadrupole-like configuration, which is a single trapping element composed of two current-carrying wires (with equal and identical-directional currents I_1) along the y-direction and a pair of anti-Helmholtz rectangular coils (with equal but opposing currents I_2) along the x-direction. In the experiments, because the cold atoms are trapped in a small central area ($\sim$ several 10μm) of the magnetic trap, only the spatial distributions of the magnetic field, gradient and its curvature within the central region of each trap are important, and the above approximation can be valid.

The magnetic field of the above quadrupole-like trap (setting a=c) can be calculated by

$$B_x = \frac{4\mu_0 I_1}{\pi} \frac{z(a^2+4x^2+4z^2)}{[(a-2x)^2+4z^2][(a+2x)^2+4z^2]}, \tag{1}$$

$$B_y = \frac{4\mu_0 I_2}{\pi} \times \frac{4aby\{a^4+(b^2-4y^2)^2-8(b^2+4y^2)z^2-48z^4+2a^2[b^2+4(y^2+z^2)]\}}{[(b-2y)^2+(a-2z)^2(b+2y)^2+(a-2z)^2][(b-2y)^2+(a+2z)^2(b+2y)^2+(a+2z)^2]}, \tag{2}$$

$$B_z = \frac{4\mu_0 I_1}{\pi} \frac{x(a^2-4x^2-4z^2)}{[(a-2x)^2+4z^2][(a+2x)^2+4z^2]} + \frac{4\mu_0 I_2}{\pi} \times \frac{4abz\{a^4+b^4+8b^2(y^2+z^2)-16(3y^2-z^2)(y^2+z^2)+2a^2[b^2-4(y^2+z^2)]\}}{[(b-2y)^2+(a-2z)^2(b+2y)^2+(a-2z)^2][(b-2y)^2+(a+2z)^2(b+2y)^2+(a+2z)^2]}, \tag{3}$$

and

$$|B| = \sqrt{B_x^2+B_y^2+B_z^2}. \tag{4}$$

Then the magnetic field distribution within the central area of each microtrap along the x-, y- and z-axes can be approximated by

$$|B(x)| = k_x \frac{4\mu_0 I_1}{\pi} \frac{|x|}{(a-2x)(a+2x)}, \tag{5}$$

$$|B(y)| = k_y \frac{4\mu_0 I_2}{\pi} \frac{ab|y|}{[a^2+(b-2y)^2][a^2+(b+2y)^2]}, \tag{6}$$

and

$$|B(z)| = k_z \frac{4\mu_0 |z|}{\pi} \sqrt{\frac{I_1^2}{(a^2+4z^2)} + \frac{16a^2b^2I_2^2}{[a^4+2a^2(b^2-4z^2)+(b^2+4z^2)^2]^2}}, \tag{7}$$

where k_x, k_y and k_z are the influence factors in the x-, y- and z-directions, which are determined by fitting the results from Eq.(4) and the calculation of the vector potential $\boldsymbol{A}$ in section 2. Using this method, we obtained k_x=1.18 for the case of 1D, 2D and 3D arrays, k_y=1.00 for the 1D array, 0.96 for the 2D array, 0.74 for the 3D array, and k_z=1.25 for the 1D and 2D arrays, 1.18 for the 3D array. It was found from our calculations that these factors (k_x, k_y and k_z) are constants and are not related to the structure parameters (a, b and c) of a current-carrying-wire array and the current I in the wires. It can be seen from these results that the current-carrying wires adjacent to each microtrap enhance the magnetic field of the quadrupole-like trap configuration (i.e. each independent trapping element) and its gradient in both x- and z-directions, while they reduce that in the y-direction. We calculated the spatial distributions (see Fig.4) of the magnetic fields in the x-, y- and z-directions from Eqs.(5), (6) and (7), and found that the results are in good agreement with the results from the calculation method used in section 2 within the limits of $\Delta x = x - x_0 = \pm a/4$, $\Delta y = y - y_0 = \pm b/4$, and $\Delta z = z - z_0 = \pm a/4$.

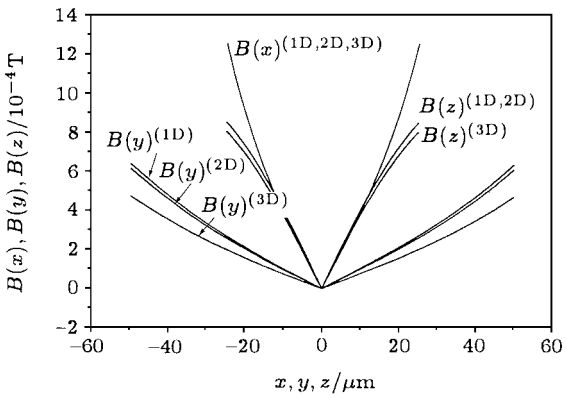


Fig.4. Spatial distribution of the magnetic field of each microscopic trap in the x-, y- and z-directions for I_1=I_2=0.2A, a=$b/2$=c=100μm. Within the central area of each microtrap, the magnetic field gradient and its curvature in the z-direction is the same as that in the x-direction.

From Eqs.(5), (6) and (7), the magnetic-field gradients in the x- and y-directions can be described by

$$\left|\frac{\mathrm{d}B(x)}{\mathrm{d}x}\right| = \frac{4\mu_0 k_x I_1}{\pi}\frac{a^2+4x^2}{(a^2-4x^2)^2}, \tag{8}$$

$$\left|\frac{\mathrm{d}B(y)}{\mathrm{d}y}\right| = \frac{16\mu_0 k_y I_2}{\pi}\frac{ab[(a^2+b^2)^2-8(a-b)(a+b)y^2-48y^4]}{[a^2+(b-2y)^2]^2[a^2+(b+2y)^2]^2}, \tag{9}$$

and the corresponding $|B|$-field curvatures in the x- and y-directions are given by

$$\left|\frac{\mathrm{d}^2B(x)}{\mathrm{d}x^2}\right| = \frac{32\mu_0 k_x I_1}{\pi}\frac{x(3a^2+4x^2)}{(a^2-4x^2)^3}, \tag{10}$$

$$\left|\frac{\mathrm{d}^2B(y)}{\mathrm{d}y^2}\right| = \frac{256\mu_0 k_y I_2}{\pi} \times \frac{aby[3(a-b)(a+b)(a^2+b^2)^2+4(3a^4+14a^2b^2+3b^4)y^2-48(a-b)(a+b)y^4-192y^6]}{[a^2+(b-2y)^2]^3[a^2+(b+2y)^2]^3}. \tag{11}$$

Since the spatial distribution of the magnetic field within the central area of each microtrap in the z-direction is similar to that in x-direction (see Fig.4), the calculation equations and results of the magnetic field gradient and its curvature in the z-direction are not shown here. It is clear from the above equations that the magnetic field of each microtrap scales as I/s, the corresponding B-field gradient and curvature scale as I/s^2 and I/s^3, respectively, where s is the characteristic size of the trap system. This shows that by using a smaller magnetic trap one can obtain a tighter confinement for cold atoms than by using a larger one, which is only limited by the practical attainable current I in the wire. From Eqs.(8)–(11), we calculated the spatial distribution of the B-field gradients and curvatures, and the results are shown in Figs.5 and 6. When I_1=I_2= 0.2A, b=2a=2c=200μm, we obtain the minimal magnetic-field gradient at the trap centre $(\mathrm{d}B/\mathrm{d}x)_{\min} \approx (\mathrm{d}B/\mathrm{d}z)_{\min} \approx 3800\times10^{-4}$T/cm, and $(\mathrm{d}B/\mathrm{d}y)_{\min} \approx 800\times10^{-4}$T/cm, and we have the maximal magnetic-field curvature $(\mathrm{d}^2B/\ \mathrm{d}x^2)_{\max} \approx 600\mathrm{T/cm}^2$ at $\Delta x = x - x_0 = \pm 25\mu$m, and $(\mathrm{d}^2B/$

$\mathrm{d}y^2)_{\max} \geq 20\mathrm{T/cm}^2$ at $\Delta y{=}y - y_0{=}\pm 50\mu$m.

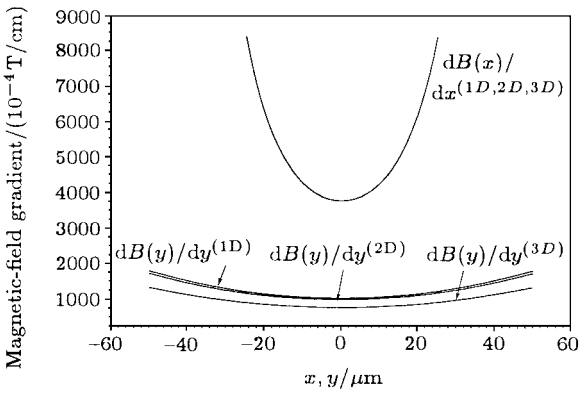


Fig.5. Spatial distribution of the magnetic field gradient of each microscopic trap in the x and y directions for $I_1{=}I_2{=}0.2$A, $a{=}b/2{=}c{=}100\mu$m. At the centre of each microtrap, the magnetic field gradient is the minimum.

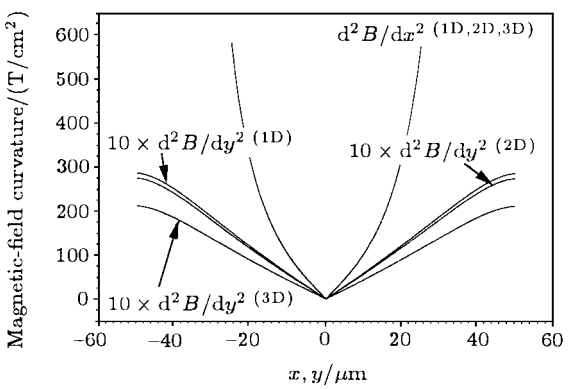


Fig.6. Spatial distribution of the magnetic field curvature of each microscopic trap in the x- and y-directions for $I_1{=}I_2{=}0.2$A, $a{=}b/2{=}c{=}100\mu$m. At the trap centre, the magnetic field curvature is equal to zero.

In consideration of the interaction between an atom with a magnetic dipole moment μ and a static, inhomogeneous magnetic field B, the trapping potential for cold atoms, due to the Zeeman effect, is position dependent and is given by

$$U_{\mathrm{Mag}} = -\boldsymbol{\mu}\cdot\boldsymbol{B} = g_{\mathrm{F}} m \mu_{\mathrm{B}} B, \qquad (12)$$

where m is the magnetic quantum number, g_{F} is the Lande g-factor, and μ_{B} is the Bohr magneton. When $\boldsymbol{\mu}\cdot\boldsymbol{B} > 0$, the trapping potential for atoms is attractive, and the atom in the strong-field-seeking state is attracted to the maximum of magnetic field. When $\boldsymbol{\mu}\cdot\boldsymbol{B} < 0$, the potential is repulsive, and the atom in the weak-field-seeking state is repulsed by the minimum of magnetic field. For ^{87}Rb atoms in the $|F{=}2, m = 2\rangle$ state, the trapping potential is $U_{\mathrm{Mag}}{=}67.2|B|\ \mu$K, where the unit of magnetic field B is the tesla. When $I{=}0.4$A, and $B(z) \geq 21\times 10^{-4}$T, we obtain $U_{\mathrm{Mag}} \geq 1.4$mK, which is far higher than the typical temperature of alkali atomic MOT (such as $\sim 120\mu$K for ^{87}Rb atoms and 240μK for ^{23}Na atoms).

4. Discussion and outlook

4.1. Loading of microtrapping arrays

To load more cold atoms within a shorter time and to obtain a higher density in each microtrap in an array of microscopic magnetic traps, we have to use a cold atomic beam to load our magnetic trap arrays. So we must first prepare a cold and intense atomic beam with a rate of $\sim 10^{10}$ atoms/s by using a 2D or 3D magnetic-optical trapping technique[19] in a lower-vacuum vapour cell. Secondly, we use a 3D optical molasses beam[20] to cool the trapped atoms in a lD or 2D array of microscopic magnetic traps, or use a 2D optical molasses beam to slow the atoms in a 3D array of microscopic traps in an ultra-high vacuum cell ($p \leq 1.333\times 10^{-9}$Pa). During the loading and cooling of cold atoms, a dense, cold atomic beam is injected into the array of current-carrying wires along the y-direction, and the currents I_1 in the wires along the y-direction are turned on, whereas the currents I_2 in the wires along the x-direction are set at a smaller value so as to generate an array of quadrupole-like fields with a suitable B-field gradient ($\sim 20\times 10^{-4}$T/cm), which will be used to form an array of microscopic MOTs. In addition, three (or two) pairs of mutually counter-propagating beams are used to cool the trapped atoms in a 1D, 2D (or 3D) array of micro-MOTs. Note that in the preparation of a 1D or 2D array of micro-MOTs, one of the 3D molasses beam axes is oriented along the horizontal y-axis and the other two beam axes are oriented along the diagonals on the xoz plane; whereas in the preparation of a 3D array of micro-MOTs, two axes of the 2D molasses beams are oriented along the y- and z-axes, respectively. In our wire arrays, the wire diameter d must be far smaller than the spacing (that is, $d \ll a, b$ and c) between two adjacent wires, usually we can choose $d \leq 0.1a$ (and $\leq 0.1b$ and $\leq 0.1c$). When a Ti:sapphire laser with a power higher than 600mW is used as a 3D (or 2D) molasses beam with a diameter of $\sim$5cm, the intensity of each beam is $\sim$10mW/cm^2, which is high enough to obtain a MOT with a number of $10^8 - 10^9$ atoms.

Next, after the 3D (or 2D) molasses beams (that is, 3D (or 2D) polarization gradient cooling) are used

to cool the cold atoms in the micro-MOT array and obtain an array of ultra-cold atomic sample with a temperature of $\sim 10\mu$K, by removing the 3D (or 2D) molasses beams and increasing the currents I_2 in the wires along the x-direction, we can realize the loading of cold atoms from an array of micro-MOTs into an array of microscopic magnetic traps. When $a = b/2 = 100\mu$m and the density of each micro-MOT is $n \approx 5 \times 10^{11}$atoms/cm^3, the trapping volume of each magnetic microtrap is $\sim 10^{-6}$cm^3, and the corresponding number of atoms trapped in each trap is about 5×10^5.

4.2. Atomic collisions and their loss rates

The collision mechanisms of cold atoms in an array of microscopic magnetic traps are similar to those in a macroscopic magnetic trap. When the atomic density n in each magnetic microtrap is higher (such as $n \approx 10^{12} - 10^{13}$atoms/cm^3), the background thermal–atom collisions, two-body spin relaxation (two-body inelastic collisions) and three-body recombination as well as non-adiabatic Majorana transitions will become four main loss mechanisms. Next we briefly discuss these loss mechanisms and estimate their loss rates.

4.2.1. Background thermal–atom collisions. This is a thermal collision between the cold ^{87}Rb atoms in the trap and the background thermal ^{87}Rb atoms in the vacuum cell. Thermal collisions can eject the trapped cold atoms out of each magnetic microtrap and result in an atomic loss. When the density of non-^{87}Rb atoms in the vacuum chamber can be neglected, the loss rate from this thermal collision can be estimated by[21]

$$\begin{cases} \gamma_{\rm BTC} = \dfrac{1}{n}\dfrac{{\rm d}n}{{\rm d}t} \approx 100 n_0 \sigma_{\rm Rb} \sqrt{\dfrac{3k_{\rm B}T}{m}}, \\ n_0 = 1.333 \times 10^{-2} \dfrac{p}{k_{\rm B}T}, \end{cases} \tag{13}$$

where p is the pressure in the vapour cell (Pa), m is the mass of a ^{87}Rb atom (kg), T is the temperature of the atomic vapour (K), $\sigma_{\rm Rb}$ is the cross section of the ^{87}Rb atom (cm^2), and n_0 is the density of background thermal ^{87}Rb atoms in the vapour cell. When p=1.333×10^{-9}Pa, T=300K and assuming $\sigma_{\rm Rb} \sim 10^{-13}$cm^2, we obtain $\gamma_{\rm ac} \approx 9.44 \times 10^{-4}$/s, the corresponding mean lifetime of ^{87}Rb atoms in the magnetic microtrap is ∼1000s.

4.2.2. Two-body spin-dipole relaxation. This is an inelastic collision between two ground-state atoms. During a collision, one or both atoms may be transited to other untrapped states due to two-body spin relaxation and then escape from the trap, which will lead to an atomic loss. The loss rate from this two-body collision is given by

$$\gamma_{\rm TBC} = \frac{1}{n}\frac{{\rm d}n}{{\rm d}t} \approx nG < 10^{-15} n \quad 1/{\rm s}, \tag{14}$$

where n is the atomic density in the trap. For ^{87}Rb atoms, $G < 10^{-15}$cm^3/s.[22] When n=10^{12} – 10^{13} atom/cm^3, we obtain $\gamma_{\rm TBC} < 10^{-3} - 10^{-2}$/s, the corresponding lifetime of atoms in each magnetic microtrap is longer than 100–1000s.

4.2.3. Three-body recombination. This is an inelastic collision among three particles. In a magnetic trap, the three-body recombination only occurs among the three ground-state atoms, its collision loss rate at the density n can be estimated by[23]

$$\gamma_{\rm TBR} = \frac{1}{n}\frac{{\rm d}n}{{\rm d}t} \approx Ln^2 \approx 4 \times 10^{-30} n^2 \quad 1/{\rm s}, \tag{15}$$

where L is the three-body recombination rate coefficient. For ^{87}Rb atoms, $L = 4 \times 10^{-30}$cm^6/s.[24] When $n = 10^{12} - 10^{13}$ atoms/cm^3, we obtain $\gamma_{\rm TBR} \approx 4 \times 10^{-6} - 4 \times 10^{-2}$/s. The corresponding lifetime of ^{87}Rb atoms in each microtrap is longer than 25s.

4.2.4. Non-adiabatic Majorana transitions. It can be seen from Figs.1, 2 and 3 that there is a point of zero B-field at the centre of each microscopic trap, which will result in an atomic loss from Majorana transitions between the trapped and untrapped states. However, since the non-adiabatic region of the quadrupole trap is so small, nearly all of the atoms will behave adiabatically.[25] This shows that only those very low energy atoms in our microtrap can escape from the centre of the quadrupole trap due to non-adiabatic processes, whereas most of trapped atoms with a temperature of $\sim 10\mu$K will stay in the trap. When the atomic temperature is equal to or higher than $\sim 10\mu$K, and $p = 1.333 \times 10^{-9}$Pa, the Majorana transitions caused by non-adiabatic motion are not likely to be observable in laser-cooled atoms.[26]

From the above analysis, we find that the dominant loss mechanism is the thermal collisions between the trapped cold atoms and background thermal atoms at lower density, such as when $n \leq 10^{12}$ atoms/cm^3, its total loss rate is less than 0.00l /s when $p = 1.333 \times 10^{-9}$Pa. When the density is higher, such as $n = 10^{12} - 10^{13}$ atoms/cm^3, both two-body spin relaxation and three-body recombination become dominant loss mechanisms in the magnetic microtraps.

4.3. Applications of magnetic microtrap arrays

It can be seen from Figs.1, 2 and 3 that there are 1D, 2D or 3D periodic magnetic-shift potentials for the trapped atoms and periodical refraction-index distribution in our magnetic microtrap arrays, like atomic optical lattices using 1D, 2D or 3D standing laser waves, so they can be used to form 1D, 2D or 3D atomic magnetic lattices (in this case, we can set a=b=c). Since there are no spontaneous emission and photon scattering effects in the magnetic lattices, and the number of atoms trapped at each lattice site can be far greater than one by using polarization-gradient cooling, this will result in a higher atomic density and a larger difference of refraction index in the magnetic lattice. Obviously, our magnetic lattices can be widely applied in the study of various magnetic trapping behaviours, nonlinear effects and wave-packet dynamics, quantum transport and tunnelling dynamics of trapped atoms as well as quantum computing with cold atoms.[27]

Moreover, when a=b=c, each microtrap in our wire arrays is a quadrupole field with a point of zero B-field at each trapped centre, which can be used to directly prepare 1D, 2D or 3D array of microscopic MOTs in a lower-vacuum vapour cell by using 3D or 2D optical molasses beams. Since the number of trapped atoms in each microtrap can reach $\sim 5 \times 10^5$ atoms, when all cold atoms from such arrays of micro-MOTs are co1lected and guided into the second MOT in an ultra-high vacuum cell by using a funnelled hollow laser beam, an alkali atomic Bose–Einstein condensation (BEC) with a higher condensed number could be realized. This shows that our arrays of micro-MOTs will have also an important application in the BEC experiment.[28]

5. Conclusions

In this paper, we have proposed several arrays of microscopic magnetic traps for cold atoms by using arrays of current-carrying wires. We have also calculated the magnetic fields of 1D, 2D or 3D arrays of microscopic magnetic traps, and analysed the magnetic field gradient and its curvature distribution of a single magnetic microtrap. The way of loading the microtrap array has been discussed, and the atomic collision mechanisms and their loss rates in each magnetic microtrap have been estimated. Finally, the potential applications of magnetic microtrap arrays in atom optics have been briefly discussed. Our study shows that by using an array of current-carrying wires with a microstructure of 10–100μm, we can form a 1D, 2D or 3D array of microscopic magnetic traps, which can be used to prepare 1D, 2D or 3D atomic magnetic lattices with a higher atomic density, or to realize 1D, 2D or 3D array of microscopic MOTs.

Compared with atomic optical lattices, since there is no spontaneous emitting nor photon-scattering effect, and a higher atomic density can be obtained in the magnetic lattices, it has more advantages and can be used to study various magnetic trapping behaviours, wave-packet dynamics, quantum transport and tunnelling dynamics of trapped atoms, and quantum computing with trapped cold atoms[27] as well as the properties of alkali atomic BEC[28,29] in atomic magnetic lattices, and so on. In particular, by using the electromagnetically induced transparence (EIT) technique,[30] the nonlinear refraction index of the trapped atomic sample in the magnetic lattice can be greatly increased, and various nonlinear magnetic lattices can be prepared and studied.

References

[1] Hemmerich A *et al* 1993 *Phys. Rev. Lett.* **70** 410
Prentiss M G 1993 *Science* **260** 1078
Collins G P 1993 *Phys. Today* **46** 17
Meacher D R 1998 *Contemporary Phys.* **39** 329

[2] Grynberg G *et al* 1993 *Phys. Rev. Lett.* **70** 2249
Hemmerich A *et al* 1994 *Phys. Rev. Lett.* **72** 625

[3] Hemmerich A *et al* 1993 *Europhys. Lett.* **22** 89
Verkerk P *et al* 1994 *Europhys. Lett.* **26** 171

[4] Meacher D R *et al* 1995 *Phys. Rev. Lett.* **74** 1958

[5] Raithel G *et al* 1997 *Phys. Rev. Lett.* **78** 630

[6] Deutsch I H *et al* 1997 *Phys. Rev.* A **56** R1705
Hemmerich A *et al* 1995 *Phys. Rev. Lett.* **75** 37

[7] Hamann S E *et al* 1998 *Phys. Rev. Lett.* **80** 4149
Vuletic V *et al* 1998 *Phys. Rev. Lett.* **81** 5768

[8] Kastberg A *et al* 1995 *Phys. Rev. Lett.* **74** 1542

[9] Rudy R *et al* 1997 *Phys. Rev. Lett.* **78** 4906
Raithel G *et al* 1998 *Phys. Rev. Lett.* **81** 3615

[10] Fischer M C *et al* 1998 *Phys. Rev.* A **58** R2648

[11] BeanDahan M *et al* 1996 *Phys. Rev. Lett.* **76** 4508

[12] Greenwood W *et al* 1997 *Phys. Rev.* A **56** 2109
Jurczak C *et al* 1996 *Phys. Rev. Lett.* **77** 1727

[13] Dutta S K *et al* 1999 *Phys. Rev. Lett.* **83** 1934

[14] Weidemuller M *et al* 1995 *Phys. Rev. Lett.* **75** 4583

[15] Kerman A J 2000 *Phys. Rev. Lett.* **84** 439
Depue M T *et al* 1999 *Phys. Rev. Lett.* **82** 2262
[16] Zabow G *et al* 1999 *Euro. Phys. J.* D **7** 351
[17] Johnson K S *et al* 1998 *Phys. Rev. Lett.* **81** 1137
Drndic M *et al* 1999 *Phys. Rev.* A **60** 4012
[18] Bergeman T *et al* 1987 *Phys. Rev.* A **35** 1535
[19] Lu Z T *et al* 1996 *Phys. Rev. Lett.* **77** 3331
Dieckinann K *et al* 1998 *Phys. Rev.* A **58** 3891
[20] Hou J D *et al* 1998 *Acta Phys. Sin.* (*Overseas Edition*) **7** 881
[21] Yin J P *et al* 1998 *Phys. Rev.* A **57** 1957
[22] Boesten H *et al* 1996 *Phys. Rev.* A **54** R29
[23] Yin J P *et al* 1998 *Opt. Commun.* **152** 421
[24] Moerdijk A J *et al* 1996 *Phys. Rev.* A **54** 916
[25] Migdall A L *et al* 1985 *Phys. Rev. Lett.* **54** 2596
[26] Metcaff H J *et al* 1999 *Laser Cooling and Trapping* (New York: Springer-Verlag) p 141
[27] Briegel H J *et al* 2000 *J. Mod. Opt.* **47** 415
[28] Yin J P *et al* 2000 *Chin. Phys.* **9** 342
[29] Yin J P *et al* 2001 *Acta Phys. Sin.* **50** 660 (in Chinese)
[30] Harris S E 1997 *Phys. Today* **50** 36